Available online at www.sciencedirect.com
ScienceDirect
Journal of Power Sources 175 (2008) 841–850
JOURNAL OF POWER SOURCES
www.elsevier.com/locate/jpowsour

Fluid dynamics performance of different bipolar plates Part I. Velocity and pressure fields

F. Barreras *, A. Lozano, L. Valiño, R. Mustata, C. Marín

LITEC/CSIC María de Luna 10, 50018 Zaragoza, Spain

Received 15 July 2007; received in revised form 7 September 2007; accepted 29 September 2007
Available online 9 October 2007

Abstract

The flow distribution obtained with three different bipolar plate geometries has been studied, analyzing their fluid dynamic performance. Three plate topologies have been selected in some way representative of different design models commonly used. The configurations tested are a set of parallel diagonal channels, a branching cascade type, and a serpentine distribution of parallel channel blocks. The flow distribution across the plates has been first simulated numerically. To visualize the flow pattern at the plate channels plane, a laser-induced fluorescence (LIF) trace tracking technique has been applied. From experimental and numerical simulations it is concluded that the diagonal topology distributes the flow in a non-uniform way. On the other hand, an inadequately large pressure drop is established along the serpentine-parallel plate. In the cascade case, both velocity and pressure fields are very uniform, and it can be expected to produce a very homogeneous distribution of reactants over the catalyst layer.

Keywords: PEM fuel cells; Bipolar plate; Fluid mechanics; Flow-field; Visualization; Modeling

1. Introduction

Fuel cells are one of the most promising technologies to face up to the growing energy demand worldwide. These devices enable a clean and efficient production of heat and power from a diversity of primary sources [1]. In hydrogen-fueled fuel cells, water is the unique byproduct generated by its electrochemical reaction with oxygen (or simply air). Based on the type of electrolyte used, fuel cells are generally divided into five categories: alkaline (AFC), proton exchange membrane (PEMFC), phosphoric acid (PAFC), molten carbonate (MCFC) and solid oxides (SOFC), which cover a wide range of operating temperatures, from less than 100 °C up to 1000 °C.

The present research is focused on proton exchange membrane (PEM) fuel cells. PEM fuel cells have been widely used since the early days of the space programs, in submarine vessels, as well as in the automotive industry. Today, the broad spectrum of applications for PEM fuel cells includes their use in portable devices such as cellular telephones or laptop computers. Even when the efficiency in energy conversion achieved in PEM fuel cells is higher than that in power plants or internal combustion engines, its optimization is dependent of a set of complex physical and chemical processes occurring simultaneously. It has been demonstrated that these processes are strongly dependent on the fuel and oxygen fluid dynamics inside the fuel cell.

Bipolar plates are singular components of PEM fuel cells because they are the first stage of the flow distribution system. The characteristics demanded for bipolar plate materials are high electrical conductivity, impermeability to gases, good thermal conductivity, lightweight, high corrosion resistance, and ease in manufacturing. Following that, bipolar plates are commonly made of graphite, some metals, or composites [2,3]. Obviously, a specific function of a bipolar plate is to produce a flow homogeneously distributed over the catalyzed electrodes. To this end some different plate geometries are typically used (squared spots, interdigitated, serpentine, spirals, etc.), as well as porous plates (porous carbon or perforated stainless steel plates). The advantages and disadvantages of some of the above flow-fields are discussed in the reviews by Carrette et al. [4], Costamagna and Srinivasan [5], and in Hertwig et al. [6]. In another research, Hontañón et al. [7] studied the gas flow distribution system of a PEM fuel cell using 3D numerical simulations, concluding that

* Corresponding author. Tel.: +34 976 716 440; fax: +34 976 716 456.
E-mail address: felix@litec.csic.es (F. Barreras).

0378-7753/$ – see front matter © 2007 Elsevier B.V. All rights reserved.
doi:10.1016/j.jpowsour.2007.09.107

Nomenclature

d	inlet duct diameter (m)
E	error in the numerical simulation
H_2	hydrogen
n	iteration number in the numerical study
v	velocity of the flow (m s^{-1} or cm s^{-1})
Re	Reynolds number
Greek symbols	
β	criteria of convergence in the numerical simulation
ν	kinematics viscosity (m^2 s^{-1})
ϕ	solution of the problem in the numerical study
ρ	density (kg m^{-3})

porous materials yielded better flow distributions compared to grooved plates, in terms of reactant gas utilization.

In a previous study, the flow distribution obtained with a parallel-channel commercial bipolar plate was analyzed using both experimental and numerical simulation techniques [8]. A non-homogeneous flow distribution across the bipolar plate surface area was observed. It was verified that the flow of gases moved preferentially along the lateral channels, as well as the presence of some channels along which the fluid circulated very slowly. This flow distribution will probably lead to an unbalanced use of the catalyst, assumed uniformly deposited, and an overall efficiency of the device lower than expected.

In this research, the same numerical and experimental techniques have been applied in order to study the flow distribution inside three different bipolar plates. The numerical code developed in [8] has been used as a tool for the design of the different geometries according to their fluid dynamics behavior. Simultaneously, flow visualization by tracking the evolution of the laser-induced fluorescence of a dyed liquid front has also been performed. Again, an excellent agreement between the numerical simulation prediction of the flow distribution in the new bipolar plates and the visualization experiments has been verified.

2. Research methodology

Bipolar plates are devices used to distribute either fuel on the anode-side or oxidizer on the cathode of PEM fuel cells. The case analyzed in this study corresponds to the flow distribution on the anode-side of a hydrogen-fueled PEM single cell. To study the different flow patterns using LIF visualization, the same experimental strategy used in [8] has been followed here, substituting the gas flow by a liquid, ensuring the dynamic similarity between the actual problem and the studied flow model. To fulfill this requirement, the same Reynolds number has to be preserved for both the gas flow and the liquid modeled one, as this dimensionless group is the one that essentially determines the fluid flow characteristics. A H_2 volumetric flow rate of 1 l min^{-1}

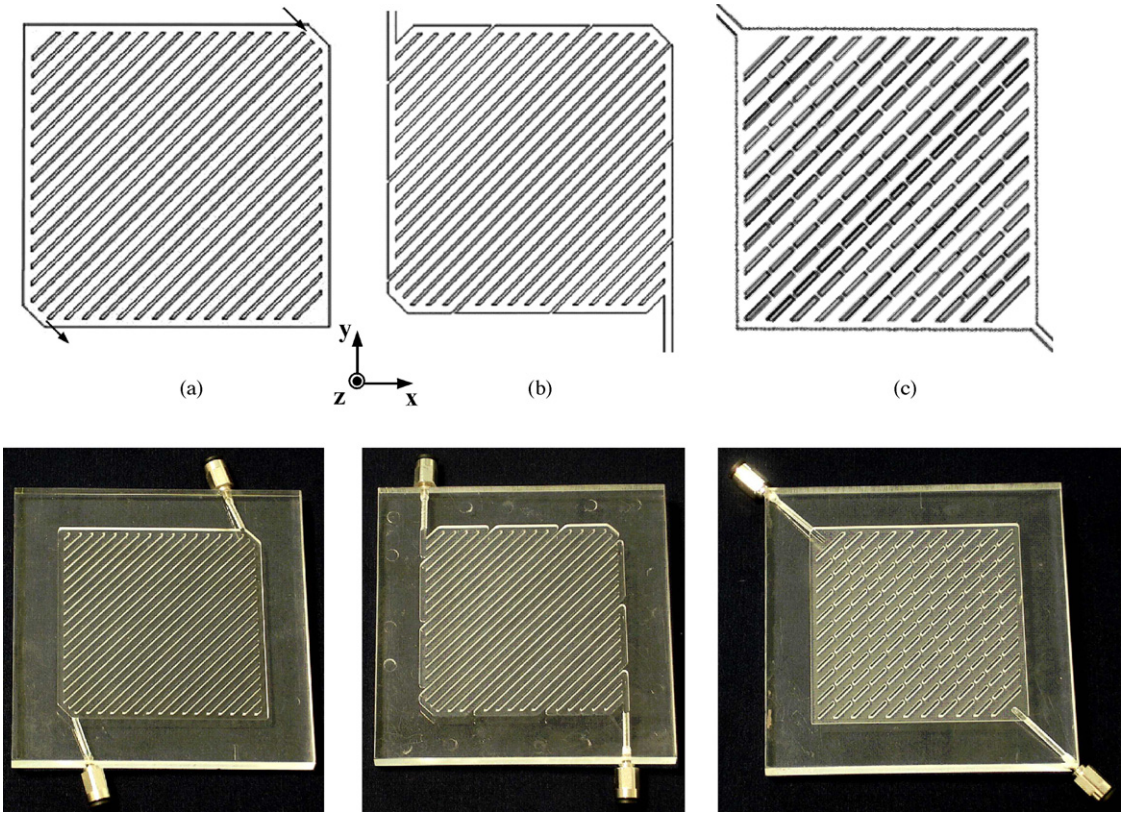

Fig. 1. Sketch and pictures of the bipolar plates used in the study: (a) diagonal, (b) parallel-serpentine, and (c) cascade.

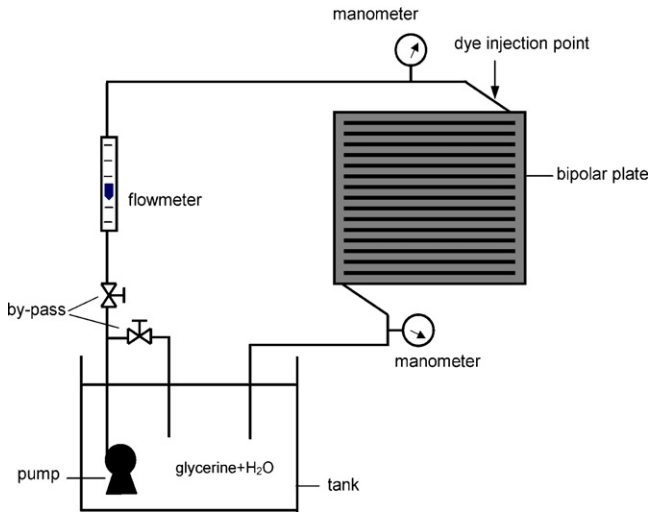

Fig. 2. Experimental facility used for visualization and velocity measurements.

(1.67×10^{-5} m^3 s^{-1}) at 80 °C has been considered. The ideal standard potential generated by a H_2/O_2 fuel cell is 1.17 V at 80 °C. A typical current density for this device would be located in a range between 400 mA cm^{-2} and 800 mA cm^{-2}. If a value of 500 mA cm^{-2} is considered, the total current for a 50 cm^2 PEM fuel cell would be 25 A. Working in the region of Ohmic polarization, for voltage values around 0.5–0.7 V the power that could be expected in a single cell configuration is about 12.5–17.5 W. Considering that, the reaction of a H_2 flow of 1 mol min^{-1} would produce a current of 3215.7 A and 25 A will result from the complete reaction of a flow of 7.77×10^{-3} mol min^{-1}. At a typical working temperature of 80 °C, this corresponds to 0.23 l min^{-1}. The selected flow rates clearly correspond to "flow-in-excess" conditions, normally used for PEM fuel cell characterization at the laboratory [9]. The main physical properties of hydrogen at 80 °C considered in the analysis [10,11] are: absolute viscosity (μ) of 1.05×10^{-5} Pa s and density (ρ) equal to 0.0674 kg m^{-3}, and a kinematic viscosity (ν) of 1.558×10^{-4} m^2 s^{-1}.

A gas entrance velocity (v_{H_2}) of 5.3 m s^{-1} results from a simple calculation for the hydrogen flow using the volumetric flow rate considered and the cross-sectional area of the inlet duct. The resulting Reynolds number ($Re = v_{H_2} d/\nu$) based on the inlet duct diameter (d) is 68. In order to perform the experiments under dynamic similarity when a liquid is used, new operational conditions have to be established to maintain the same Reynolds number. As in [8], a mixture of glycerin/water with 49.6% of glycerin and 51.4% of water (in volume) has been selected. This mixture, after perfectly stirred, is transparent, and the fluorescent dye can easily be dissolved in it. The resulting kinematic viscosity of the mixture, measured with a Rheotest viscosimeter at ambient temperature, is 24.1 cSt (24.1×10^{-6} m^2 s^{-1}). Then, for a Reynolds number of 68, a volumetric flow rate of 230 ml min^{-1} is required, which corresponds to an entrance velocity of 1.22 m s^{-1} for the glycerin/water mixture.

2.1. Numerical code

The 2D computer code used as a tool for the designing procedure of the different flow-field topologies is based on the steady Navier–Stokes conservation equations for mass and momentum, namely

$$\nabla(\rho\vec{v}) = 0 \tag{1}$$

$$\nabla(\rho\vec{v}\cdot\vec{v}) = -\nabla p + \nabla(\mu\nabla\vec{v}) + \rho\vec{g} \tag{2}$$

The numerical analysis has been performed for an X–Y plane according to the coordinate axis defined in Fig. 1, slicing all the channels in the plate in their middle section. To discretize the coupled Navier–Stokes equations, a finite volume method [12] has been preferred over finite elements, given the simple geometrical topologies selected for the bipolar plates. Finite differences scheme has been discarded due to its non-conservative character. A regular Cartesian staggered grid has been used in order to improve the velocity–pressure coupling. This coupling is numerically implemented using a SIMPLE [13] algorithm. Finally, a gradient-conjugate technique has been applied to iteratively solve the resulting linear equation system.

A thorough discussion about the simplification of the problem to a two-dimensional approach in the numerical simulation can be found in [8]. To accommodate the 2D numerical simulation to the 3D physical problem is essential to preserve the Reynolds number at the inlet duct. The actual 3D flow rate (Q_{3D}) imposes a 2D flow rate (Q_{2D}) given through the relationship

$$Q_{3D} = \frac{\pi}{4} d Q_{2D} \tag{3}$$

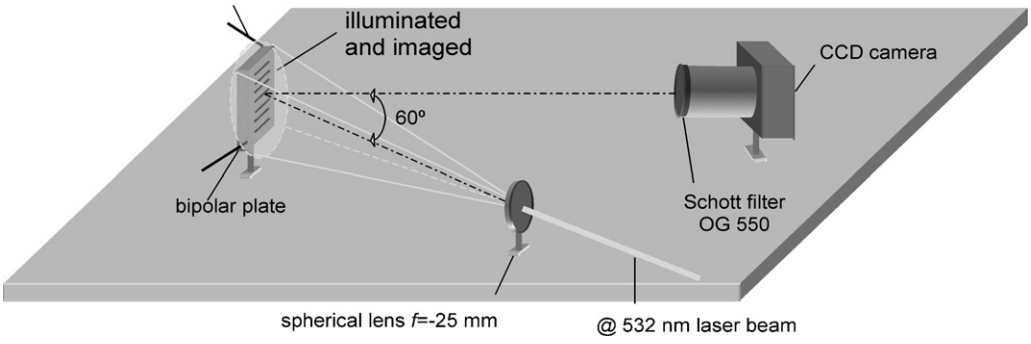

Fig. 3. Optical setup arranged for flow visualization.

So, for an actual volumetric flow of 230 ml min^{-1} and a Reynolds number of 68, the corresponding 2D flow rate is 2.44×10^{-3} m^2 s^{-1}, with the same inlet velocity (1.22 m s^{-1}) obtained from the non-dimensional analysis.

A 138×138 grid has been selected to discretize the flow region in all plates, because it has a spatial resolution high enough to simulate with a good precision the flow conditions in the bipolar plates. Comparisons between the numerical simulations and the experimental results previously performed in [8] for the commercial parallel-channel bipolar plate showed that for 50,000 iteration steps, a level of convergence, β, on the order of 10^{-20} is obtained for this discretization grid. This coefficient β is defined in the following way: assuming that the solution after each iteration behaves as a Cauchy series, an error can be defined associated to each iteration as

$$E_0 = |\phi_1 - \phi_0| \geq |E_1 = |\phi_2 - \phi_1| \geq \cdots \geq E_n = |\phi_{n+1} - \phi_n| \geq \cdots \geq 0 \quad (4)$$

Extending the previous idea to define an error associated between two levels of iteration, using the triangle inequality,

$$|\phi_{n_2} - \phi_{n_1}| \leq |\phi_{n_2} - \phi_{n_2-1}| + \ldots + \phi_{n_2} - \phi_{n_2-1}| \leq |n_2 - n_1||\phi_2 - \phi_1| \quad (5)$$

it is obtained,

$$E_{n_2-n_1} \equiv \frac{|\phi_{n_2} - \phi_{n_1}|}{|n_2 - n_1||\phi_2 - \phi_1|} \quad (6)$$

This is a non-dimensional error with values between 0 and 1. A criteria or level of convergence β is reached when

$$E_{n_2-n_1} \leq \beta \ \ \forall x \quad (7)$$

The level of convergence, β, of an order of 10^{-20} seems very accurate, corroborating the validity of the 2D approximation used in the numerical simulation. It has also been noted that in the former study the velocity solution in the last channels of the commercial plate took longer to converge. This was physically explained because of the close presence of the outlet duct that causes a slower setting of a proper pressure field at its exit. To minimize errors due to this influence, the first 5 mm of the exit pipe have been included in the simulation domain for all the plates.

Although the flow is steady, the numerical scheme requires an initial condition to start the simulation. A constant (in modulus) small velocity has been considered through all the channels. The numerical value has been chosen to preserve mass conservation.

2.2. Bipolar plate configurations

The configurations of the new plate geometries have been proposed considering the main conclusions derived from the analysis of the flow distribution of the parallel-channel commercial one [8], trying to avoid some of the observed drawbacks. For example, it was verified that strong re-circulating bubbles were forming at the central channels entrance because they were placed at a right angle with respect to the lateral channels. As a consequence, the effective flow area becomes dramatically reduced, blocking the fluid entrance to the channels. For this reason, a 45° angle between the longitudinal channels and the lateral ones has been considered in all the bipolar plate topologies designed for the present study.

The experiments have been performed in three different plates, as depicted in Fig. 1, designed as an alternative to the parallel-channel commercial one used in both single and stack

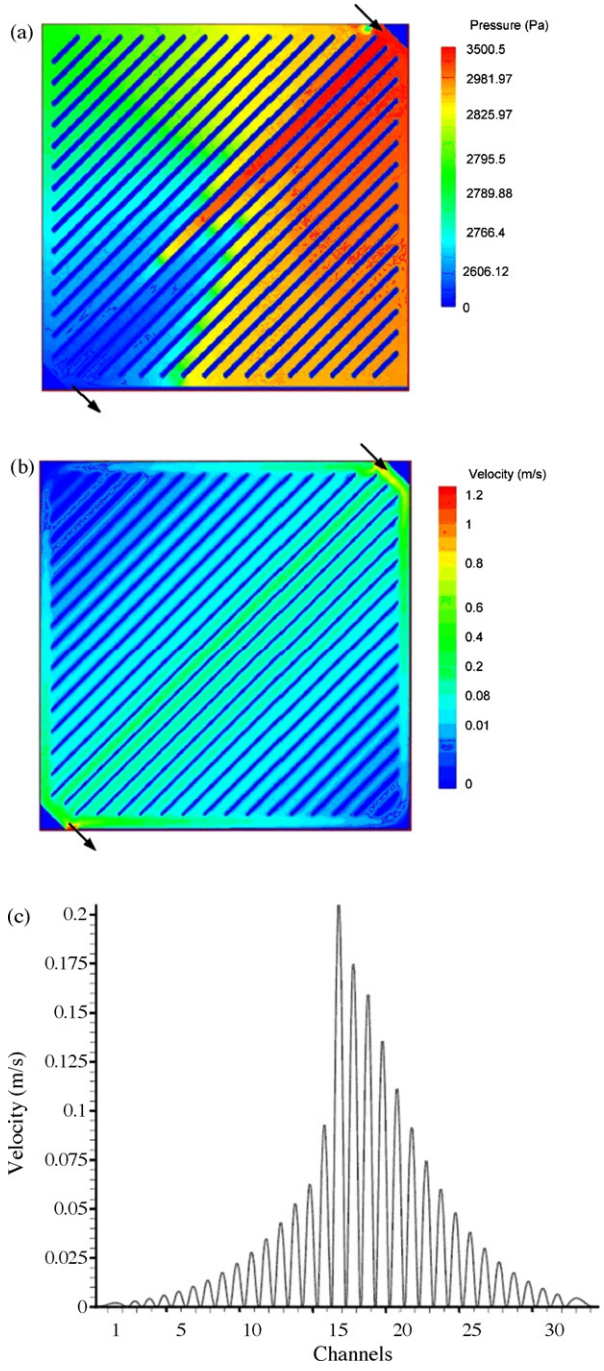

Fig. 4. Numerical simulation results obtained for the diagonal-type configuration: (a) pressure field, (b) velocity field, and (c) average velocity values along the plate diagonal.

fuel cell devices, and that are representative of frequently used topologies. So, the 7 $cm^2 \times 7\ cm^2$ active area, the diameter of inlet and outlet ducts (2 mm), the width of the lateral channels (2 mm), and the depth of the channels (1 mm) have been maintained in the new alternatives. The rest of parameters (number of channels, thickness of the ribs, and the width of the channels) have been properly re-dimensioned. All bipolar plates have been machined in transparent plastic to ease the experimental visualization of the flow pattern.

The diagonal-type bipolar plate is formed by 32 channels, with a width of 2 mm, separated by 1 mm thick ribs (see Fig. 1(a). A similar configuration has been considered for the serpentine-parallel plate, as depicted in Fig. 1(b), arranging the 32 channels in 11 blocks. In this case, inlet and outlet ports have also been moved to suitable locations. The cascade flow-field bipolar plate is shown in Fig. 1(c), consisting of 20 longitudinal channels 3.1 mm wide, separated by ribs with a thickness of 1 mm. In this last configuration the perpendicular flow area connecting one channel to the next one has been maintained constant and equal

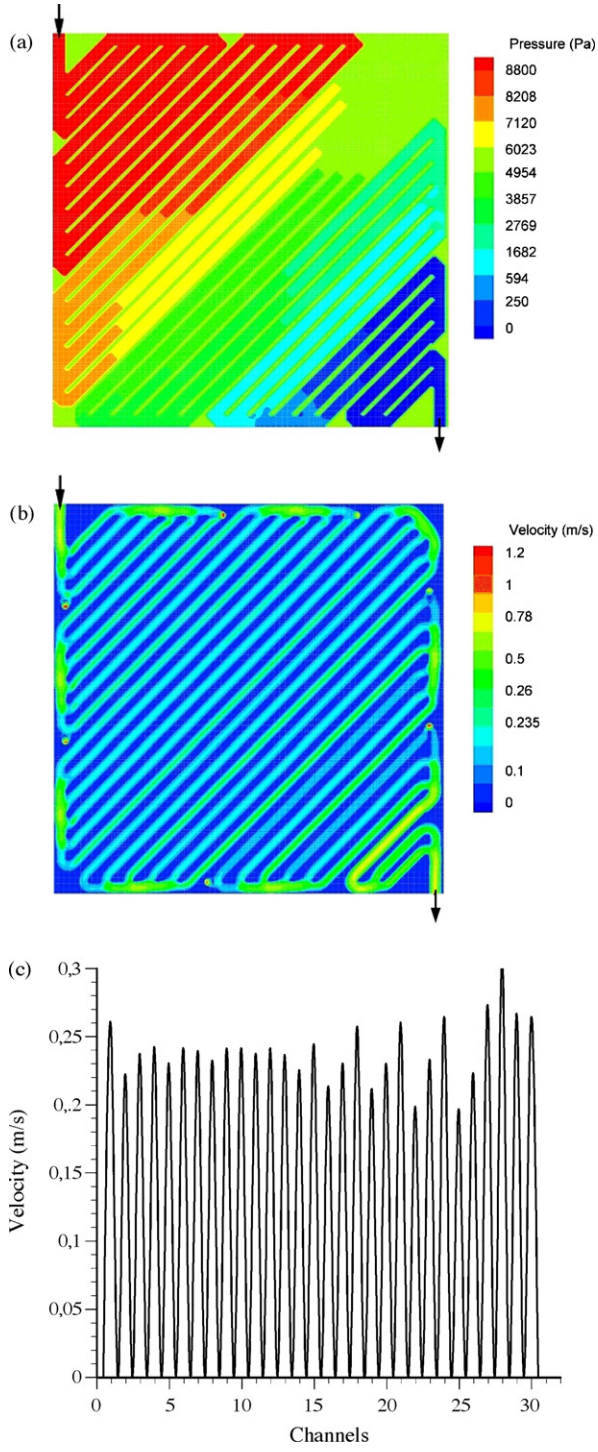

Fig. 5. Numerical simulation results obtained for the serpentine-parallel bipolar plate: (a) pressure field, (b) velocity field, and (c) average velocity values along the plate diagonal.

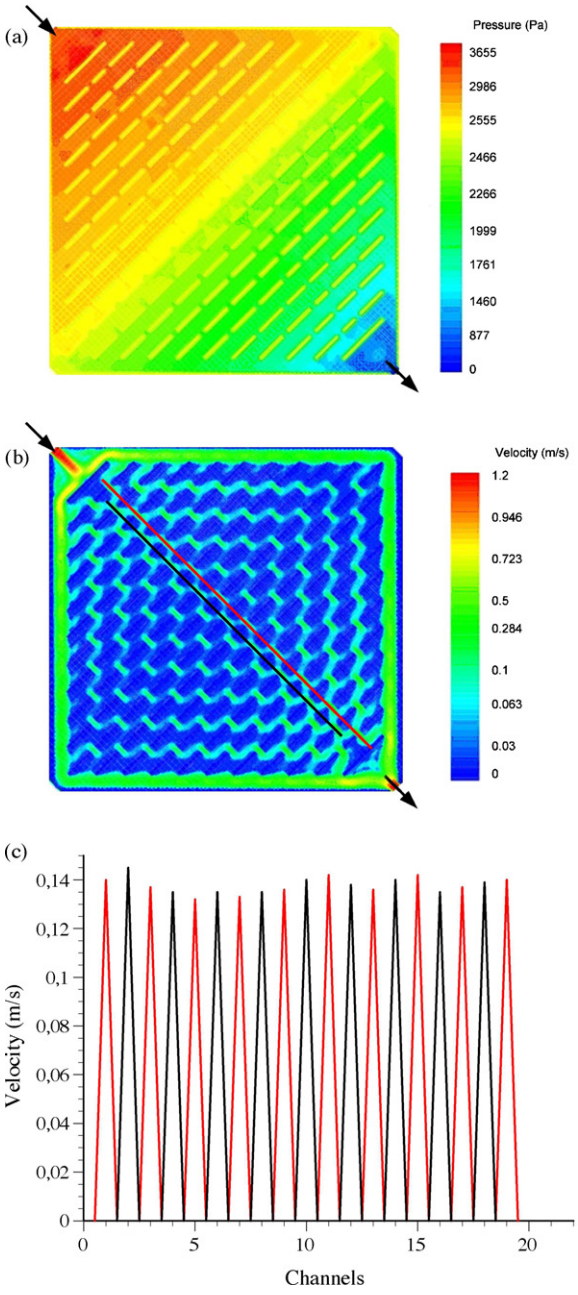

Fig. 6. Numerical simulation results obtained for the branching cascade bipolar plate: (a) pressure field, (b) velocity field, and (c) average velocity values corresponding to the two lines depicted in (b).

to the cross sectional area of the inlet duct. So, the number and width of the slits on each rib change from one to another. In all cases, quick connectors have been placed at the inlet and outlet ducts in order to ease the experimental assembly procedure.

2.3. Experimental facilities

The experimental facility used in the experiments of this research is displayed in Fig. 2. It includes the bipolar plate assembly, a 10 l tank, an immersion pump capable of supplying a maximum flow rate of 100 l min^{-1}, two manometers and a flowmeter with a maximum reading of 1.7 l min^{-1}, and an accuracy of 0.03 l min^{-1}. A by-pass has also been included before the bipolar plate position to avoid large pressure drops and, hence, liquid overheating. The dye injection point is placed 80 mm (40 diameters) upstream of the inlet point, and consists of a 1 mm capillary welded at an angle of 45° with respect to the axis of the inlet duct. The front-face of the experimental model consists of a transparent plastic cover that seals the bipolar plate. Before circulating the glycerin/water mixture, some preliminary tests using water were performed to check the correct sealing. Besides, the temperature variation of the fluid at the reservoir was continuously measured to evaluate the efficiency of the by-pass system. Before acquiring the images, the liquid was allowed to circulate during 5 min ensuring stationary flow conditions. After this time, dye was injected in pulses,

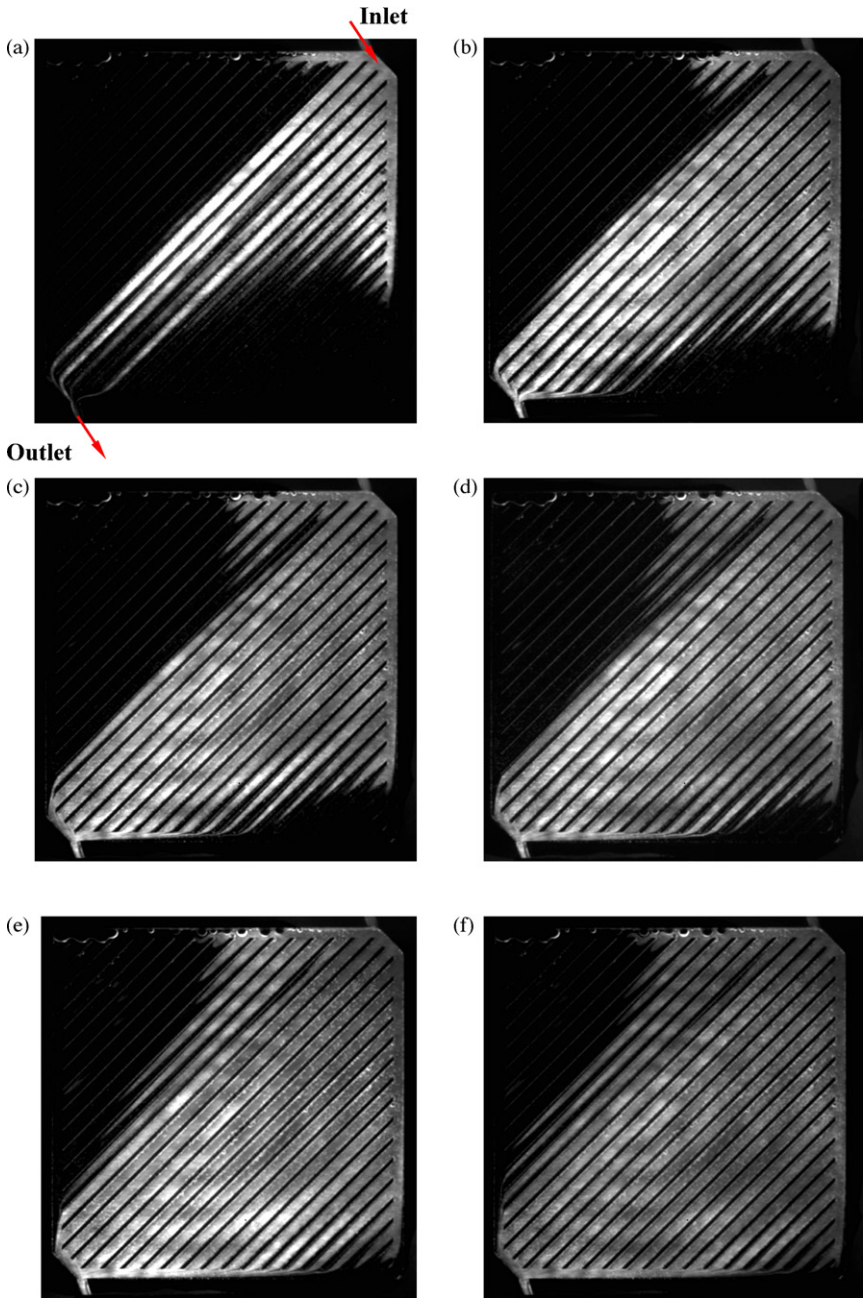

Fig. 7. Temporal sequence showing the evolution of the dyed fluid for the diagonal-type plate: (a) 0.5 s, (b) 1 s, (c) 1.5 s, (d) 2 s, (e) 4.5 s, and (d) 5 s.

synchronized with the laser pulses and the image acquisition system, controlled by a DG-535 Stanford Research Pulse Delay Generator.

To visualize the flow pattern, laser-induced fluorescence (LIF) has been applied, using sulforhodamine B (Kiton red) dissolved in the water/glycerin mixture as the luminescent tracer. To excite the dye, a double cavity Quantel YG781C-10 pulsed Nd:YAG laser has been used, doubling the frequency of its emission to obtain an energy of 100 mJ per pulse at 532 nm, with a pulse duration of 6 ns. This excitation scheme is very efficient for this tracer because the absorption spectrum of sulforhodamine B has a maximum at 556 nm [14]. The emitted fluorescence light is in the orange range, with the peak at 620 nm. To further decrease the background light recorded, a Schott OG 550 filter has been placed in front of the camera lens, blocking any 532 nm reflection from the incident laser beam.

To image the fluorescence emission, an interlined Hamamatsu ORCA-ER 1024×1024 pixels CCD camera has been used, placed perpendicular to the bipolar plate. As depicted in Fig. 3, a spherical lens with a focal distance of -25 mm has been placed at 1 m of the bipolar plate to expand the laser beam obtaining a slightly divergent cylinder of light, which illumi-

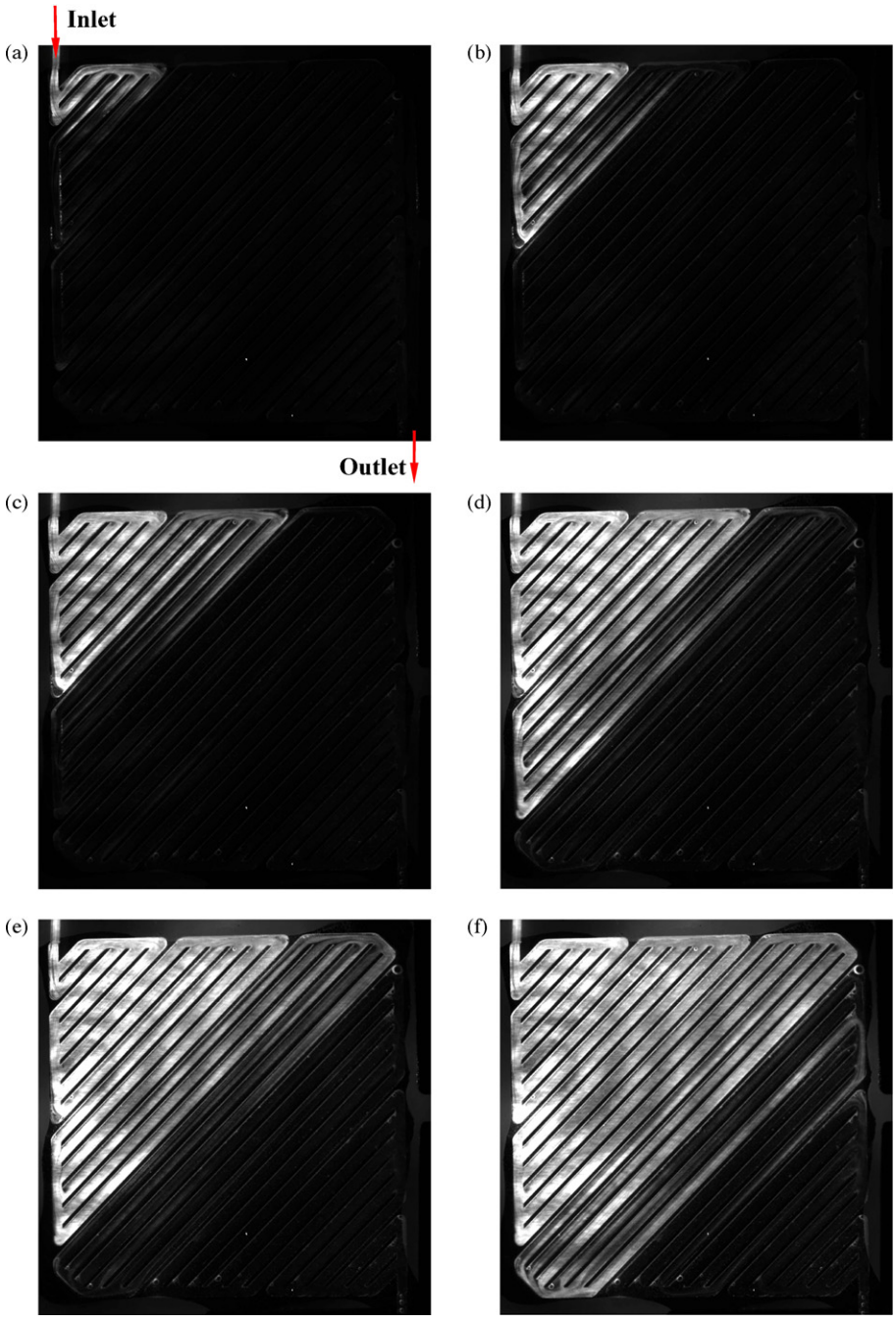

Fig. 8. Temporal sequence showing the evolution of the dyed fluid for the parallel-serpentine plate, for the same time intervals as in Fig. 7.

nates the plate at an angle of 60° with respect to the axis of the camera. This arrangement does not introduce any perspective distortion in the images and eliminates any possible direct reflection of the laser light that might damage the CCD camera. Data sets have been recorded with a 50 mm *f*# 1.2 Nikon lens, giving a field of view of 72 mm × 72 mm with a spatial resolution of 70.3 μm pixel^{-1}. To track the evolution of the dye front, several sequences of ten images have been acquired for every bipolar plate configuration for a constant flow of 230 ml min^{-1}, setting the time interval between successive images at 0.5 s. However, it has to be noted that for the serpentine-parallel case, the actual flow rate was limited by the high-pressure drop.

3. Results

The velocity magnitude and pressure fields obtained for the three configurations analyzed in the present study are depicted in Figs. 4–6. An uneven flow distribution can be expected when experimentally testing the diagonal topology. As can be observed in Fig. 4(c), large velocity values are predicted for the flow that moves along the central channels. Simultaneously, it is also observed that the flow is not symmetrically distributed, tending to circulate preferentially in the lower area of the plate. On the contrary, a very homogeneous velocity field is obtained for both the serpentine-parallel and the cascade-type flow topologies, as can be observed in Figs. 5 and 6. Velocity profiles depicted in

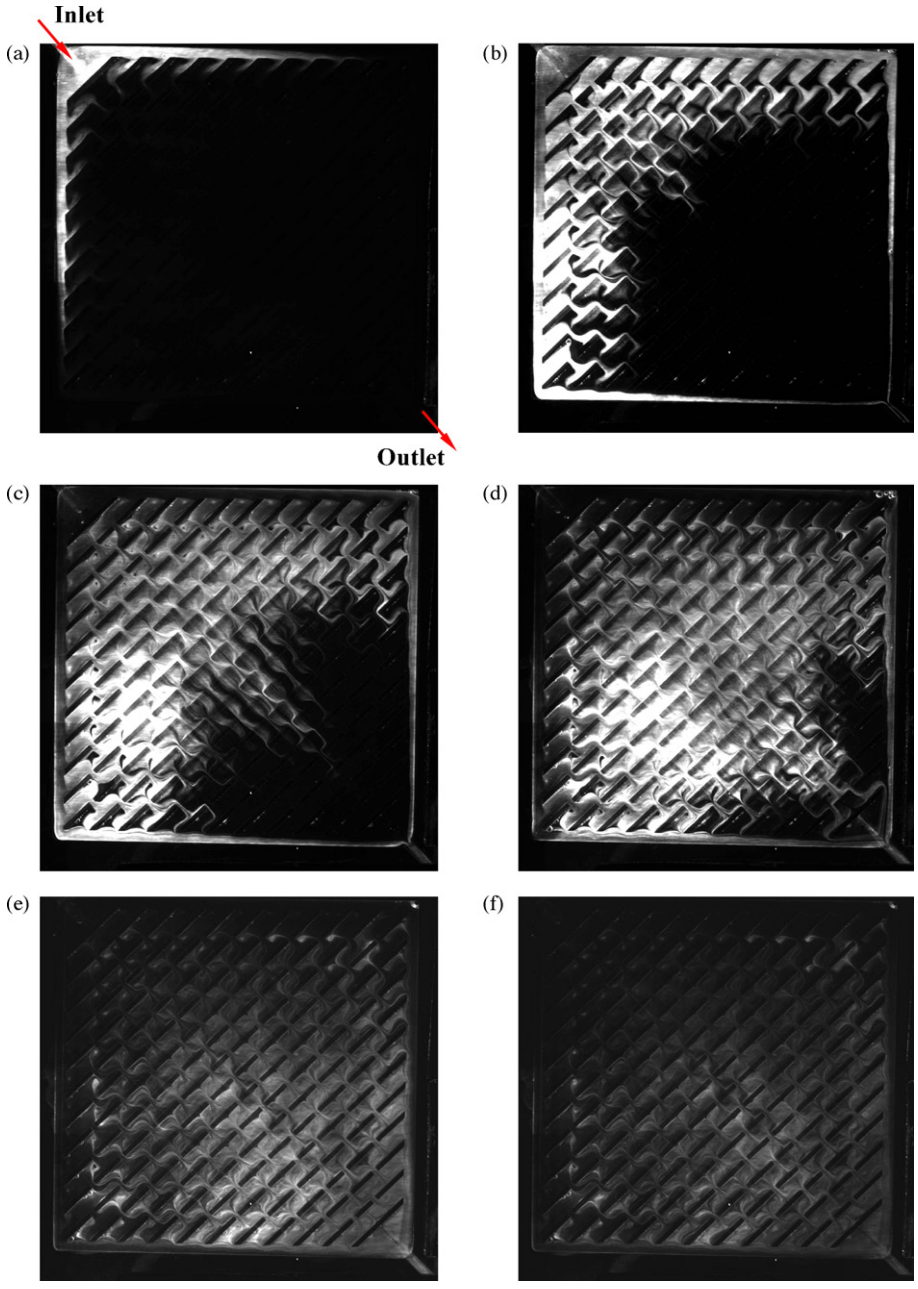

Fig. 9. Temporal sequence showing the evolution of the dyed fluid for the cascade-type bipolar plate, for the same time intervals as in Fig. 7.

Figs. 4(c) and 5(c), correspond to the plate diagonal, while the graph plotted in Fig. 6(c) shows the velocities along the two lines indicated in Fig. 6(b). Another significant result is the large maximum pressure values obtained for the serpentine-parallel configuration, roughly 2.5 times higher than those obtained for the other two bipolar plates. On the other hand, the cascade-type plate yields a flow homogeneously distributed in the whole plane, with a roughly constant pressure drop along the different longitudinal channels.

Some examples of the flow distribution obtained from the experimental study can be observed in the sequences of images displayed in Figs. 7–9 corresponding to the diagonal, serpentine-parallel, and cascade flow topologies, respectively. The temporal evolution of the dye front progressing across the plates can be easily observed. To ease the analysis only the images corresponding to 0.5 s, 1 s, 1.5 s, 2 s, 4.5 s, and 5 s after the seeding of each sequence have been selected. The flow distribution produced by the diagonal bipolar plate configuration is presented in the sequence at Fig. 7 and, as predicted by the numerical simulation study, a highly non-uniform flow distribution is observed. As can be seen in the first image, the flow tends to move preferentially along the central channels. A large area at the upper part of the plate almost depleted of any dye trace is observed in the subsequent images, indicating that the flow circulates with a very low velocity in that zone. Finally the dyed fluid is mostly concentrated in the lower part of the plate, giving a non-symmetric flow distribution, in good agreement with the velocity and pressure fields predicted by the numerical simulation.

The other two configurations distribute homogeneously the flow with an almost constant velocity field. Fig. 8 shows the image sequence corresponding to the parallel-serpentine flow-filled plate. In the selected sequence, a constant dye seeding has been applied during the recording time to keep illuminated the whole area behind the initial front of dye. Even so, 5 s after the start of the experiment, corresponding to the last image in the sequence, the dyed-fluid fills only two-thirds of the flow area, approximately. This behavior indicates that the large pressure drop-induced for this bipolar plate configuration on the liquid flow, is causing a decrease in the volumetric flow rate. On the other hand, an almost flat advance of the dye front is obtained in the cascade-type bipolar plate, as can be observed in Fig. 9(c) and (d). As can also be noticed, just 1.5 s after the start of the sequence (Fig. 9(c)), fresh fluid is already entering the plate, diluting the trailing edge of the dyed-fluid, and evidencing an increase in the volumetric flow rate. It is for this reason that the total intensity of the emitted fluorescence light of the last two images of the sequence is proportionally low. This result also corroborates the low-pressure drop introduced by this flow-field configuration, and the homogeneous pressure field produced as predicted by the numerical simulation performed.

Finally, it is important to note that the velocity field of the different bipolar plates studied will probably be modified when the flow across the gas diffusion layer (GDL) is considered. The flow through the GDL will depend on the pressure field in the bipolar plate and consequently, uniformity of the velocity field (flow distribution) along the channels of the plates might not be the condition to ensure a concentration of reactants homogeneously distributed over the catalyst layer. It is for this reason that we can, for example, expect that, even when the velocity field obtained for the serpentine-parallel bipolar plate is homogeneous, the concentration of gases over the catalyst layer will be non-uniformly distributed. A large amount of hydrogen (or oxygen) will probably flow through the area close to the entrance, where the pressure difference across the GDL is higher, as shown from the numerical simulation analysis in Fig. 5(a). This situation will produce a decrease on the overall efficiency of the fuel cell.

4. Conclusions

Three different bipolar plates, in some way representative of different design models commonly used, with an electrode-side area of 49 cm^2 have been numerically and experimentally studied: a set of parallel diagonal channels, a branching cascade type, and a serpentine distribution of parallel-channel blocks. Numerical simulations performed reveal the importance of both pressure and velocity fields on the fluid dynamic behavior for a given configuration. It has been verified that the diagonal-type bipolar plate tested yields a non-uniform flow distribution for both the velocity and pressure fields. In this configuration the flow tends to move preferentially by the central channels, and a non-symmetric flow distribution across the plate plane has also been detected. The serpentine-parallel plate distributes the flow with a uniform velocity field, but with an excessively large pressure drop. On the other hand, a flow homogeneously distributed is obtained with the cascade-type flow geometry, together with a quite uniform pressure field over the whole plate.

In the second part of this research, the influence of the different flow-field bipolar plate configurations on the flow distribution behind the gas diffusion layers typically used in PEM fuel cells will be analyzed. It is expected that the relative importance of both velocity and pressure fields will be highlighted.

Acknowledgements

This research has been partially supported by the Spanish Education and Science Ministry under the project ENE2005-09124-C04-03/ALT, the Aragon Government under the project PM042/2007 and by the Network of Fuel Cell Batteries of the Spanish Council for Scientific Research (CSIC).

References

[1] Hydrogen, Energy and Fuel Cells—A Vision for our Future, High Level Group for Hydrogen and Fuel Cells, Summary Report, June 2003.
[2] F. Barbir, J. Braun, J. Neutzler, J. New Mater. Electrochem. Syst. 2 (1999) 197–200.
[3] V. Mehta, J.S. Cooper, J. Power Sources 114 (2003) 32–53.
[4] L. Carrette, K.A. Friedrich, U. Stimming, Fuel Cells 1 (1) (2001) 5–39.
[5] P. Costamagna, S. Srinivasan, J. Power Sources 102 (2001) 253–269.
[6] K. Hertwig, L. Martins, R. Harwoth, Fuel Cells 2 (2) (2002) 61–77.
[7] E. Hontañón, M.J. Escudero, C. Bautista, P. García-Ybarra, L. Daza, J. Power Source 86 (1/2) (2000) 363–368.

[8] F. Barreras, A. Lozano, L. Valiño, C. Marin, A. Pascau, J. Power Source 144 (1) (2005) 54–66.
[9] Personal communication with researchers of the National Institute of Aerospatial Technique (I.N.T.A.) of Spain.
[10] R.H. Perry, D.W. Green, J.O. Maloney, Perry's Chemical Engineers Handbook, 6th ed., McGraw-Hill, 1984.
[11] F.M. White, Fluid Mechanics, McGraw-Hill, USA, 1979.
[12] J.H. Ferziger, M. Peric, Computational Methods for Fluid Dynamics, 2nd Rev ed., Springer-Verlag, Berlin, 1999.
[13] S.V. Patankar, Numerical Heat Transfer and Fluid Flow, McGraw-Hill, New York, USA, 1980.
[14] U. Brackmann, Lambdachrome Laser Dyes, Lambda Physik GmbH, Göttingen, Germany, 1994, pp. 160–161.